The influence of Ca doping on the crystal structure and superconductivity of orthorhombic $YBa_2Cu_3O_{7-\delta}$

1996 J. Phys.: Condens. Matter 8 8889

(http://iopscience.iop.org/0953-8984/8/45/021)

J. Phys.: Condens. Matter **8** (1996) 8889–8905. Printed in the UK

The influence of Ca doping on the crystal structure and superconductivity of orthorhombic $YBa_2Cu_3O_{7-\delta}$

G Böttger†, I Mangelschots‡, E Kaldis‡, P Fischer†, Ch Krüger‡ and F Fauth†

† Laboratory for Neutron Scattering, ETH Zurich & Paul Scherrer Institute, 5232 Villigen PSI, Switzerland

‡ Laboratory for Solid State Physics, ETH Hönggerberg, 8093 Zürich, Switzerland

Received 20 June 1996, in final form 20 August 1996

Abstract. The changes of the chemical structure of $YBa_2Cu_3O_{7-\delta}$ ($\delta < 0.04$) and of the superconducting transition temperature T_c associated with Ca doping have been investigated by means of neutron and x-ray powder diffraction, oxygen content determination and magnetic susceptibility measurements. In this work, we were able to show that the depression of superconductivity in Ca-substituted orthorhombic $YBa_2Cu_3O_{7-\delta}$ is related to essential structural changes. Using the cation–oxygen distances obtained by neutron diffraction at 1.5 K we calculated the bond valence sums of the cations. This allows us to estimate the charge distribution within the structure and yields a direct correlation between structural changes induced by Ca doping and T_c. Our results show clearly that Ca doping leads to an overdoping of $YBa_2Cu_3O_{7-\delta}$ which cannot be reached by oxygen non-stoichiometry alone.

1. Introduction

It is well known that the oxygen stoichiometry and oxygen defect structure are crucial quantities determining the occurrence or suppression of superconductivity in the perovskite-type compounds $RBa_2Cu_3O_{7-\delta}$ (R denotes Y and most rare earths). The oxygen stoichiometry dependence of T_c has been explained in terms of a charge transfer from the chains to the planes [1], leading to an increase of the hole concentration in the superconducting CuO_2 planes. Charge transfer is of course also achieved by doping, e.g., by substitution of Ca^{2+} for R^{3+}. Ca substitution in the Y–Ba–Cu–O family leads to different effects. While in $YBa_2Cu_4O_8$ ('124') T_c can be increased up to 90 K by Ca substitution at predominantly Y sites [2] as proven directly with single-crystal diffractometry [3], in $Y_2Ba_4Cu_7O_{15-\delta}$ ('247') where Y and Ba are partially substituted for with Ca, no influence on T_c has been detected [4]. Interestingly, in $YBa_2Cu_3O_{7-\delta}$ ('123') two effects occur with Ca doping: the tetragonal, oxygen-poor phase ('$123O_6$') becomes superconducting with $T_c \approx 50$ K [5], whereas in the orthorhombic, oxygen-rich phase ('$123O_7$') contradictory trends for T_c are reported in the literature. No change of T_c with Ca substitution is reported in [6], while in [7] a decrease of T_c was found. Moreover many of the reported results concerning structural aspects of the Ca substitution in 123 are contradictory. With increasing Ca content of orthorhombic 123 samples, e.g. for the lattice parameter c an increase in reference [4], a decrease in reference [6] and no change in references [7, 8] are reported. Even the assertation that Ca substitution in $YBa_2Cu_3O_{7-\delta}$ produces overdoping of the material is disputed; see e.g. references [8] or [9] and [10].

0953-8984/96/458889+17$19.50

In order to clarify the behaviour of orthorhombic $YBa_2Cu_3O_{7-\delta}$ under Ca doping, we have synthesized a series of 12 powder samples with Ca contents from 0% to 20% and performed a series of oxygen content, DC susceptibility, x-ray and high-resolution ($\Delta d/d \geqslant 2 \times 10^{-3}$, d = lattice spacing) neutron powder diffraction measurements. Section 2 provides a description of the experimental techniques and the data analysis. In section 3 the main results of these measurements are presented. In section 4, the links between the evolution of the crystallographic structure and the superconducting properties are discussed.

2. Experimental details and data analysis

Polycrystalline samples with nominal composition $Y_{1-x}Ca_xBa_2Cu_3O_{7-\delta}$ ($0 \leqslant x \leqslant 0.20$; $\delta < 0.04$) were prepared by solid-state reaction. Stoichiometric mixtures of high-purity powders of Y_2O_3, $CaCO_3$, $BaCO_3$ and CuO were mixed in ethanol by means of a ball mill and subsequently dried for one day. The powder was subsequently annealed at temperatures of 860, 870 and 885 °C for 16 hours in air. Then further annealing was performed in flowing oxygen at 900 °C (8 h), 920 °C (8 h), 940 °C (70 h) and 960 °C (30 h) in order to expel the carbonate traces. To maintain a high oxygen content and a homogeneous oxygen distribution all of the samples were ground thoroughly in between annealings and finally cooled in oxygen with a very slow cooling rate of 4 °C h^{-1} from 500 °C. The polycrystalline samples were characterized by powder x-ray diffraction using Ge(111)-monochromatized Cu Kα radiation (STOE-STADI P) at room temperature. Measurements were carried out in transmission mode between 5° and 120° with 2θ steps of 0.2° (each step 80 s). Additionally, neutron diffraction experiments were performed at the high-flux reactor at the Institute Laue–Langevin (Grenoble). In this work, the D1A diffractometer ($\lambda \simeq 1.908$ Å) was used for a precise structure determination in particular of the oxygen positions. The neutron powder diffraction patterns were recorded at 1.5 K in a 2θ angular range between $-6°$ and 159° with 2θ steps of 0.05°.

The Rietveld method was used to refine the crystallographic structure. For refining the x-ray powder diffraction data we used the program STADI P [11]. All neutron diffraction data were analysed with the program FullProf [12], which allows the simultaneous treatment of several phases. The background was described by a polynomial of second order. The Thompson–Cox–Hastings pseudo-Voigt function was used to describe the profile and the full width at half-maximum (FWHM) of the Bragg reflections. Due to the smallness of some of the structural changes, special attention was paid to analysing the data in a consistent way. For the structure refinement we used data collected in the range $10.4° \leqslant 2\theta \leqslant 155.45°$.

All of the bond lengths have been calculated with the program Bondstr of J Rodríguez-Carvajal. Due to the higher sensitivity of neutrons compared to that of x-rays as regards detecting oxygen atoms we used our neutron diffraction data for calculating bond lengths. The cation–oxygen distances were taken to estimate the oxidation state (chemical valence) of Cu at the different sites, and consequently the number of holes in the CuO_2 plane. The bond valence sums V_i for the cations in $Y_{1-x}Ca_xBa_2Cu_3O_{7-\delta}$ were calculated as well with the program Bondstr using the following equation given in references [13, 14]:

$$V_i = \sum_j s_{ij} = \sum_j \mathrm{e}^{(Ro_i - R_{ij})/B_i} \tag{1}$$

where V_i is the oxidation state of cation i and s_{ij} the valence (or strength) of the bond between the cation i and the anion j. Ro_i and B_i are constants whose values have been tabulated for many bond types [14]. In our case, R_{ij} are the cation–oxygen distances obtained by neutron diffraction at 1.5 K.

For characterization of superconducting properties, the DC magnetic susceptibility was measured using a SQUID magnetometer in the field-cooling mode in an external field of about 0.0024 T between 5 and 120 K.

The oxygen content of all of the polycrystalline samples was determined both by a very sensitive volumetric method [15] and by neutron diffraction.

3. Results

3.1. Structural aspects

X-ray and neutron powder diffraction data indicate that all of the samples up to a Ca concentration of 17% are single-phase materials. Only the sample with a higher Ca content ($x = 20\%$) showed a small amount of $BaCuO_{2+\delta}$ (less than 0.5%) which suggests that the solubility limit is near the 20% composition.

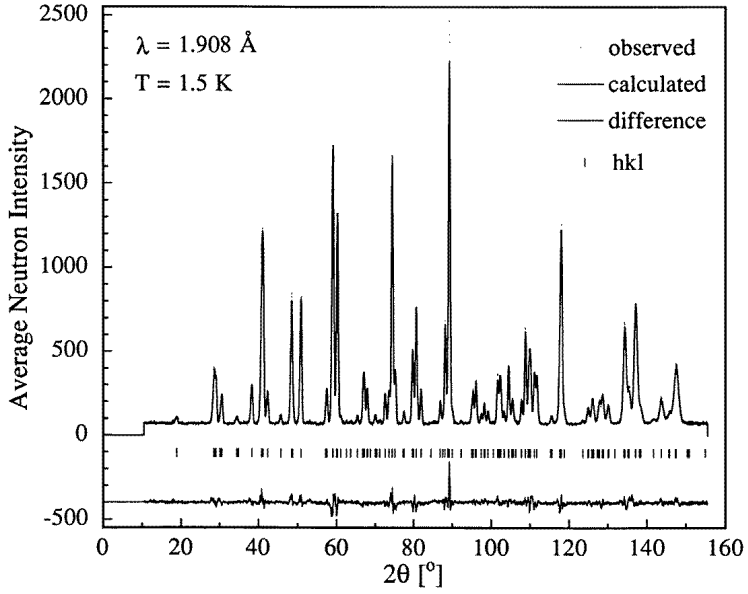

Figure 1. Observed, calculated and difference neutron powder diffraction patterns of $Y_{0.91}Ca_{0.09}Ba_2Cu_3O_{7-\delta}$ measured on D1A at 1.5 K.

The crystallographic structure of all $Y_{1-x}Ca_xBa_2Cu_3O_{7-\delta}$ samples was refined on the basis of the space group *Pmmm*. The corresponding structural parameters are given in table 1. Note that the quoted errors do not include the uncertainty in the effective neutron wavelength. As a typical example figure 1 shows the neutron diffraction pattern of $Y_{0.91}Ca_{0.09}Ba_2Cu_3O_{7-\delta}$ measured on the D1A diffractometer in a standard vanadium container. We see that the agreement between the observed and calculated patterns is good.

The substitution for yttrium with calcium up to a Ca content of 20% could be verified by structure refinements of both neutron and x-ray powder diffraction data. With the Rietveld structure refinement method no evidence was found for the suggestion that Ca may be located at Ba sites [4, 16]. This is an unambiguous result since we have used both neutron and x-ray powder diffraction. Using x-ray diffraction one gets an excellent contrast between

Table 1. Structural parameters at 1.5 K for $Y_{1-x}Ca_xBa_2Cu_3O_{7-\delta}$ ($\delta < 0.04$) with various Ca stoichiometries x. The relative cell dimensions a, b, c are reliable within the quoted standard deviations, but these do not include the uncertainty in the effective neutron wavelength $\lambda = 1.907\,97(5)$Å.

x		0	0.02	0.04	0.05	0.07	0.09
δ		0.06(1)	0.09(1)	0.07(1)	0.06(1)	0.09(1)	0.08(1)
a (Å)		3.81154(5)	3.81294(6)	3.81239(7)	3.81201(6)	3.81383(7)	3.81241(7)
b (Å)		3.88137(7)	3.88094(8)	3.87982(9)	3.87915(9)	3.88015(9)	3.87753(9)
c (Å)		11.6477(2)	11.6489(2)	11.6546(3)	11.6556(3)	11.6574(3)	11.6564(3)
V (Å^3)		172.32(1)	172.38(1)	172.39(1)	172.36(1)	172.51(1)	172.31(1)
s		9.08	8.84	8.77	8.73	8.62	8.47
R_{wp} (%)		5.23	6.33	5.07	6.07	5.97	6.29
R_{exp} (%)		3.21	3.40	4.22	3.56	3.45	3.82
χ^2		2.66	3.47	4.66	2.91	2.99	2.71
R_B (%)		3.21	3.24	3.94	3.22	4.25	3.21
Y/Ca	B (Å^2)	0.26(4)	0.29(4)	0.48(4)	0.24(4)	0.50(4)	0.34(4)
Ba	z/c	0.1833(2)	0.1839(2)	0.1842(2)	0.1839(2)	0.1840(2)	0.1842(2)
	B (Å^2)	0.05(4)	0.25(4)	0.30(4)	0.16(4)	0.14(4)	0.19(4)
Cu(1)	B (Å^2)	0.18(5)	0.22(5)	0.15(6)	0.20(5)	0.42(6)	0.17(5)
Cu(2)	z/c	0.3542(1)	0.3544(1)	0.3547(1)	0.3543(1)	0.3544(1)	0.3546(1)
	B (Å^2)	0.14(3)	0.27(3)	0.36(3)	0.41(4)	0.25(3)	0.28(3)
O(1)	z/c	0.1595(2)	0.1597(2)	0.1599(2)	0.1594(2)	0.1591(2)	0.1591(2)
	B (Å^2)	0.35(4)	0.49(4)	0.45(5)	0.41(4)	0.55(5)	0.46(4)
O(2)	z/c	0.3784(2)	0.3780(2)	0.3778(2)	0.3780(2)	0.3780(2)	0.3776(2)
	B (Å^2)	0.33(4)	0.45(4)	0.57(4)	0.41(4)	0.36(4)	0.44(4)
O(3)	z/c	0.3771(2)	0.3775(2)	0.3778(2)	0.3772(2)	0.3768(2)	0.3768(2)
	B (Å^2)	0.30(4)	0.38(4)	0.54(4)	0.34(4)	0.37(4)	0.39(4)
O(4)	n	0.90(1)	0.86(1)	0.87(1)	0.89(1)	0.88(1)	0.87(1)
	B (Å^2)	0.1(1)	0.2(1)	0.4(1)	0.3(1)	0.3(1)	0.4(1)
O(5)	n	0.04(0)	0.05(0)	0.06(0)	0.05(0)	0.03(0)	0.05(0)
	B (Å^2)	0.1(1)	0.2(1)	0.4(1)	0.3(1)	0.3(1)	0.4(1)
x		0.10	0.12	0.14	0.15	0.17	0.20
δ		0.09(3)	0.10(1)	0.06(1)	0.09(1)	0.09(2)	0.09(2)
a (Å)		3.81431(9)	3.81355(8)	3.81340(7)	3.81296(8)	3.8140(1)	3.8148(1)
b (Å)		3.8788(1)	3.8761(1)	3.8769(1)	3.8753(1)	3.8744(1)	3.8723(1)
c (Å)		11.6608(4)	11.6571(3)	11.6659(3)	11.6638(3)	11.6731(4)	11.6722(4)
V (Å^3)		172.52(1)	172.31(1)	172.47(1)	172.35(1)	172.49(2)	172.42(2)
s		8.38	8.14	8.25	8.10	7.86	7.48
R_{wp} (%)		6.80	6.17	5.33	6.40	6.45	6.53
R_{exp} (%)		4.13	3.43	3.63	3.64	3.90	3.77
χ^2		2.71	3.23	2.16	2.84	2.79	3.00
R_B (%)		6.03	3.97	2.82	3.07	4.80	3.46
Y/Ca	B (Å^2)	0.44(5)	0.31(4)	0.51(5)	0.29(4)	0.57(5)	0.27(4)
Ba	z/c	0.1841(3)	0.1842(2)	0.1846(2)	0.1849(2)	0.1855(2)	0.1852(2)
	B (Å^2)	0.06(6)	0.27(5)	0.20(4)	0.28(4)	0.12(5)	0.33(5)
Cu(1)	B (Å^2)	0.53(8)	0.13(6)	0.41(6)	0.17(6)	0.42(6)	0.23(6)
Cu(2)	z/c	0.3542(2)	0.3547(1)	0.3545(1)	0.3549(1)	0.3549(1)	0.3551(1)
	B (Å^2)	0.03(4)	0.22(3)	0.30(3)	0.31(3)	0.30(3)	0.34(3)
O(1)	z/c	0.1588(2)	0.1592(2)	0.1589(2)	0.1591(2)	0.1582(2)	0.1588(2)
	B (Å^2)	0.42(6)	0.54(5)	0.50(5)	0.55(5)	0.71(5)	0.65(5)
O(2)	z/c	0.3778(3)	0.3773(2)	0.3776(2)	0.3776(2)	0.3777(2)	0.3772(2)
	B (Å^2)	0.20(5)	0.41(4)	0.47(4)	0.47(4)	0.43(4)	0.40(4)
O(3)	z/c	0.3760(3)	0.3768(2)	0.3763(2)	0.3763(2)	0.3762(2)	0.3758(2)
	B (Å^2)	0.22(5)	0.39(4)	0.44(4)	0.45(4)	0.43(4)	0.49(4)
O(4)	n	0.87(2)	0.85(1)	0.89(1)	0.85(1)	0.87(1)	0.83(1)
	B (Å^2)	0.2(1)	0.4(1)	0.6(1)	0.6(1)	0.7(1)	0.8(1)
O(5)	n	0.04(1)	0.05(0)	0.05(0)	0.06(0)	0.04(1)	0.08(1)
	B (Å^2)	0.2(1)	0.4(1)	0.6(1)	0.6(1)	0.7(1)	0.8(1)

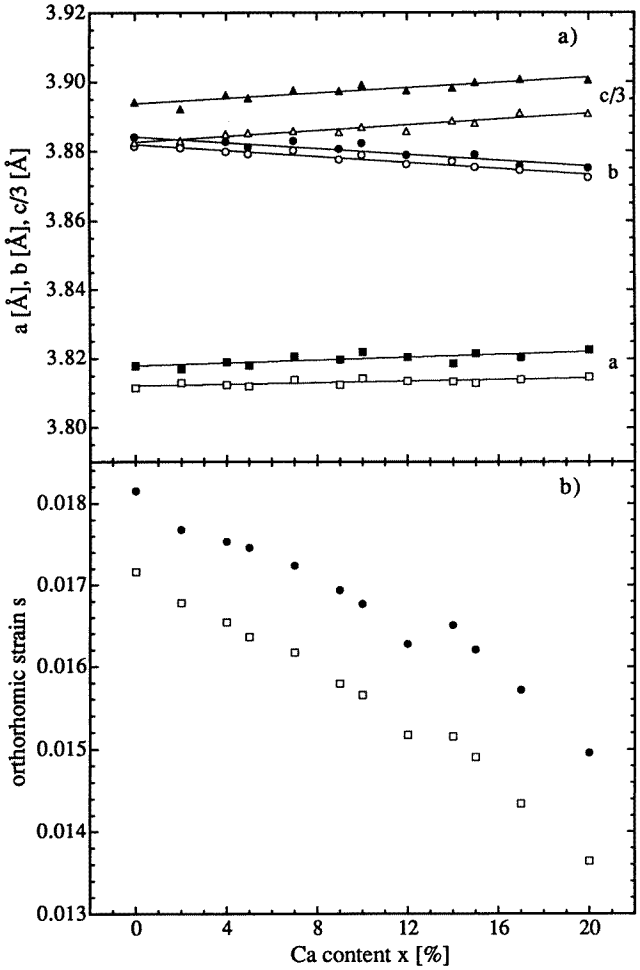

Figure 2. (a) Lattice parameters of $Y_{1-x}Ca_xBa_2Cu_3O_{7-\delta}$ ($\delta < 0.04$), a (squares), b (circles) and $c/3$ (triangles), determined by x-ray diffraction at room temperature (full symbols) and by neutron diffraction at 1.5 K (open symbols). The error bars are in all cases smaller than the size of the points. The lines are linear fits. (b) The orthorhombic strain of $Y_{1-x}Ca_xBa_2Cu_3O_{7-\delta}$ determined by x-ray diffraction at room temperature (squares) and by neutron diffraction at 1.5 K (cycles).

Ca and Ba atoms since the numbers of electrons for Ca ($Z = 20$) and Ba ($Z = 56$) are quite different. The contrast between Y ($Z = 39$) and Ca is sufficient. Thus a direct determination of the Ca distribution is possible by x-ray diffraction. With neutron diffraction one gets a good contrast between Y and Ca atoms due to the bound coherent neutron scattering lengths $b_c(\mathrm{Y}) = 7.75$ fm and $b_c(\mathrm{Ca}) = 4.70$ fm. On the other hand, a direct determination of the Ca distribution on Ba sites is not possible by neutron diffraction due to the rather similar b_c-values of Ca and Ba atoms: 4.70 fm and 5.07 fm, respectively [17]. However, our results do not exclude the possibility of a Ca substitution on both the Y and Ba sites at Ca concentrations higher than our maximum Ca content of 20% . The Ca substitution on both the Y and Ba sites at a Ca content lower than 20% might be possible for different

synthesis conditions such as those used for our polycrystalline samples prepared by solid-state reaction. In the case of using a sol–gel method, quenching the samples from 500 °C or growing single crystals from a flux, the value for the Ca concentration at which a substitution for both the Y and the Ba sites possibly starts might differ [18]. We also note here that a partial substitution for Ba^{2+} seems to take place in single crystals of Ca-124 with higher Ca content [19].

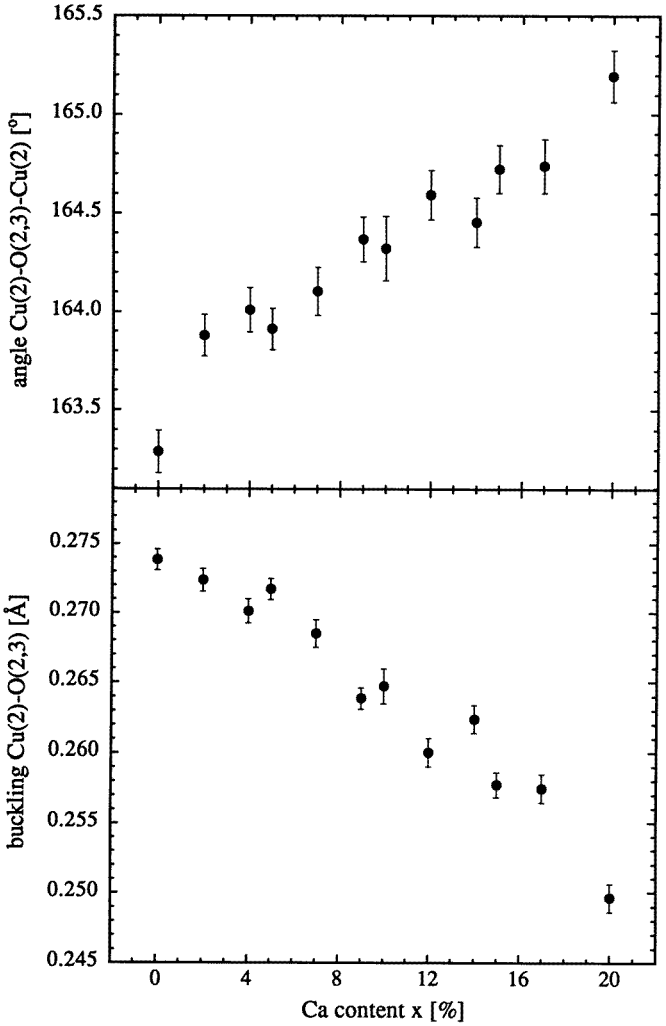

Figure 3. Buckling of the CuO_2 plane of $Y_{1-x}Ca_xBa_2Cu_3O_{7-\delta}$ represented by the angle Cu(2)–O(2, 3)–Cu(2) (a) and the distance between the plane copper Cu(2) and the averaged oxygen layer O(2,3) of the CuO_2 plane (b). The buckling of the CuO_2 plane is defined as: $k = c[\frac{1}{2}(z_{O2} + z_{O3}) - z_{Cu2}]$. All of the data shown in this plot were determined from neutron diffraction data at 1.5 K.

The Ca incorporation in the orthorhombic phase of 123 leads to the following structural changes.

(1) The lattice constants *a* and *c* increase while *b* is decreasing (figure 2(a)).

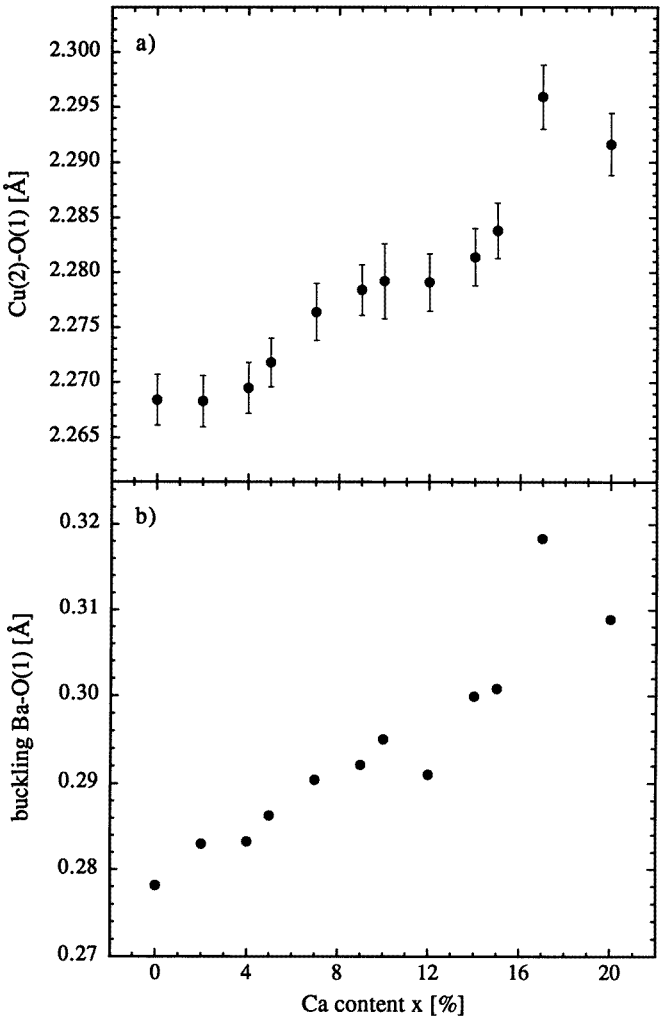

Figure 4. (a) The apical bond length Cu(2)–O(1) of $Y_{1-x}Ca_xBa_2Cu_3O_{7-\delta}$ as a function of the Ca content at 1.5 K. (b) Buckling of the Ba–O(1) plane of $Y_{1-x}Ca_xBa_2Cu_3O_{7-\delta}$ as a function of the Ca content x. Buckling of the Ba–O(1) plane is defined as: $k = c(z_{Ba} - z_{O1})$. All of the data shown in this plot have been determined from neutron diffraction data at 1.5 K. The error bars (estimated standard deviations) are smaller than the size of the points.

(2) The unit-cell volume increases slightly.

(3) The orthorhombic strain s, a measure of the length difference between the a- and b-axes, decreases linearly (figure 2(b)). The orthorhombic strain s is defined as

$$s = \frac{2(b-a)}{a+b}. \tag{2}$$

(4) The order of the single Cu–O chains decreases, i.e. the occupancy of the O(4) position is decreasing, while the occupancy of the 'off-chain' O(5) position is increasing.

(5) The fractional z/c-coordinate of the apical oxygen O(1) is decreasing; this ion is shifted away from the CuO_2 plane towards the basal plane, a typical behaviour for a decrease

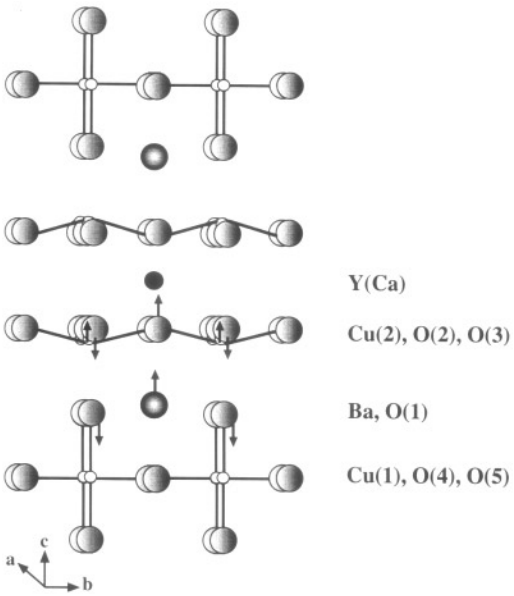

Figure 5. The structure of $YBa_2Cu_3O_{7-\delta}$. Atoms building the CuO single chains and atoms building the CuO_2 planes are connected with solid lines. Arrows indicate the atomic displacements induced by Ca substitution.

of T_c in the Y–Ba–Cu–O family.

(6) In the CuO_2 plane the buckling is diminished (figure 3), which is reflected in an increasing Cu(2)–O(2, 3)–Cu(2) angle. This is combined with a shift of Cu(2) away from the single chain, and therefore

(7) the Cu(2)–Cu(2) distance decreases.

(8) The Cu(2) and apical oxygen O(1) are moving mutually away from each other, and hence the apical bond length Cu(2)–O(1) is increasing (figure 4(a)).

(9) The fractional z/c-coordinate of the Ba^{2+} ion is increasing; this ion is shifted away from the basal plane towards the CuO_2 plane. Consequently, the distance Y(Ca)–Ba decreases while Ba–O(4) increases.

(10) As a consequence of (9) the distances Ba–O(2) and Ba–O(3) decrease.

(11) Resulting from the mutual movement of the Ba ion and of the apical oxygen O(1) away from each other, the buckling of the Ba–O(1) layer increases (figure 4(b)).

(12) The distances Y(Ca)–O(2) and Y(Ca)–O(3) increase.

Figure 5 displays the structure of $YBa_2Cu_3O_{7-\delta}$; the atomic displacements occurring with Ca substitution are indicated by arrows.

Results of the oxygen content determination are given in table 2. We can see that the oxygen content determined for samples with $x > 4\%$ is higher than the nominal value, which was calculated by assuming an average copper valence of 2.33. Moreover, the oxygen content decreases with Ca doping in good agreement with the results reported by Greaves and Slater [7]. This fact suggests that the reduction in oxygen content is due to a charge balance associated with substitution for Y^{3+} with Ca^{2+} and an effect of an increasing oxidation state of copper cations which will be discussed later. We note, however, that the oxygen content in [7] was estimated only by TGA. The aspects concerning the dependence of many properties of Ca-123 on the oxygen content determined are discussed elsewhere [20].

Table 2. Comparison of calculated oxygen content and by a volumetric method determined oxygen content of $Y_{1-x}Ca_xBa_2Cu_3O_{7-\delta}$ ($\delta < 0.04$).

	Calculated oxygen content δ^{calc} for an average copper valence of		Oxygen content determined	
x (%)	+2	+2.33	δ^{exp}	$\delta^{\text{calc}}(Cu^{2.33+}) - \delta^{\text{exp}}$
0	6.500	7.000	6.995(2)	−0.005(2)
2	6.490	6.990	6.967(2)	−0.023(2)
4	6.480	6.980	6.980(2)	± 0.000(2)
5	6.475	6.975	6.979(2)	+ 0.004(2)
7	6.465	6.965	6.981(2)	+ 0.016(2)
9	6.455	6.955	6.976(2)	+ 0.021(2)
10	6.450	6.950	6.963(2)	+ 0.013(2)
12	6.440	6.940	6.963(2)	+ 0.023(2)
14	6.430	6.930	6.975(2)	+ 0.045(2)
15	6.425	6.925	6.960(2)	+ 0.035(2)
17	6.415	6.915	6.960(2)	+ 0.045(2)

3.2. Magnetic properties

Field-cooled magnetization measurements were performed between 5 and 120 K in a field of 0.0024 T on powdered samples. The superconducting transition temperature T_c was defined at 90% of the superconducting transition width since the transition width varies slightly with Ca doping. However, a different definition of T_c would not change any of the observed trends. In table 3 the values for T_c and the superconducting volume fraction V_{SC} (Meissner) are given. Figure 6(a) shows T_c plotted as a function of Ca concentration x in $Y_{1-x}Ca_xBa_2Cu_3O_{7-\delta}$. We observed a decrease of T_c as the Ca doping level was increased. The depression rate of T_c is approximately −1.6 K/at.% for Ca substitution. The magnitude of the Meissner component of the magnetization is also reduced significantly with Ca concentration. Moreover, we found a dependence of T_c on the buckling of the CuO_2 planes (figure 6(b)). This correlation is of significance since it has been found for R-123 compounds (R = rare-earth elements) that a critical buckling angle of about 167.3° exists at which the superconductivity disappears [21]. The highest buckling angle in our samples is reached for 20% Ca concentration.

Table 3. Values for T_c and the superconducting volume fraction V_{SC} (Meissner).

x (%)	T_c (K)	$V_{SC}(T_c)$ (%)
0	88	95
2	87	69
4	83	69
5	80	72
7	78	80
9	74	66
10	71	55
12	72	77
15	62	60
20	56	52

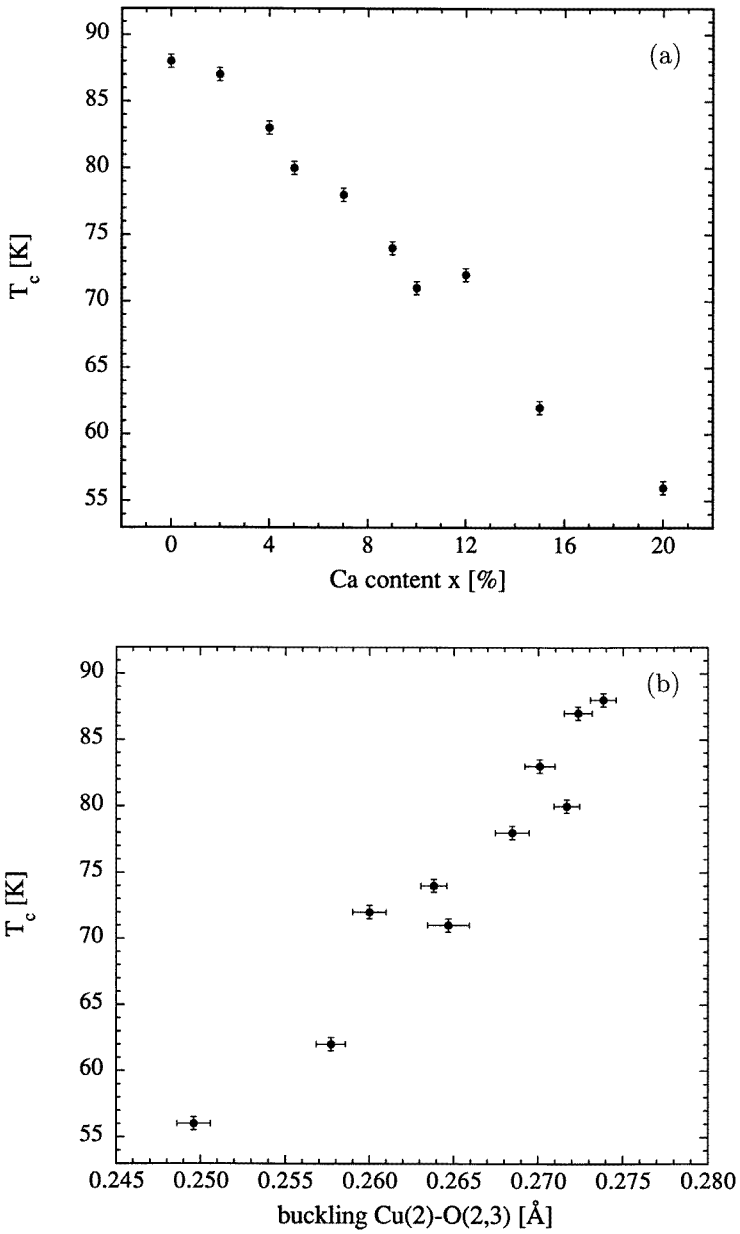

Figure 6. The superconductive transition temperature T_c as a function of the Ca content x of $Y_{1-x}Ca_xBa_2Cu_3O_{7-\delta}$ (a) and as a function of the buckling of the CuO_2 plane (b).

3.3. Calculation of the bond valence sum (BVS)

We have calculated the bond valence sums (BVS) around all of the atoms in our $Y_{1-x}Ca_xBa_2Cu_3O_{7-\delta}$ series from equation (1). The results are shown in table 4 together with one data set obtained for $x = 0$ given in reference [22]. Whereas most values from reference [22] are less than 2% different from the data calculated with BVS for our sample

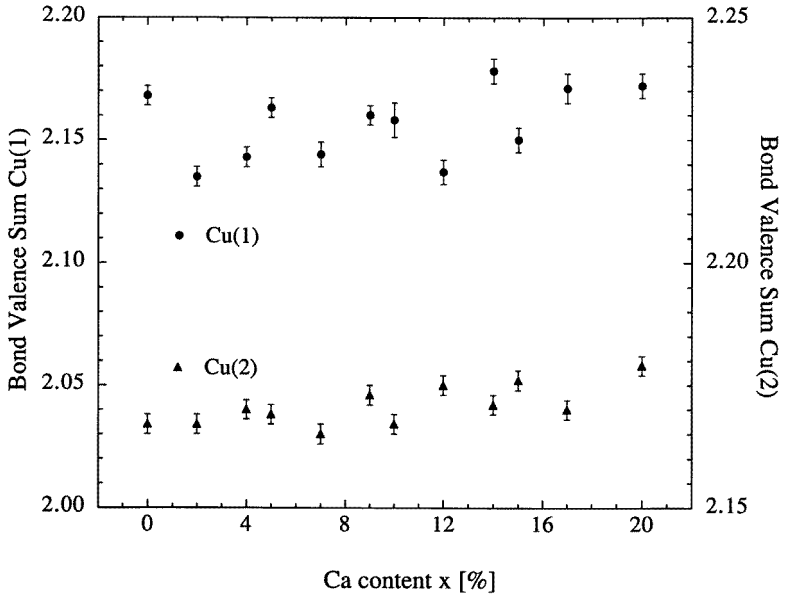

Figure 7. Bond valence sums around chain coppers Cu(1) and plane coppers Cu(2) as a function of the Ca content x of $Y_{1-x}Ca_xBa_2Cu_3O_{7-\delta}$.

with $x = 0$, there is a 10% difference in the BVS for Cu(1). This difference can be explained by the different coordination spheres in these samples. In reference [22] Cu(1) has been assumed to be coordinated only by O(1) and O(4) atoms while in our sample an additional, partially occupied 'off-chain' O(5) site was found in the coordination sphere of Cu(1). This 'splitting' of oxygen is possibly the result of the slow cooling of our samples. The previous samples [23] were quenched. The values of the bond valence sum around the planar and chain coppers are shown in figure 7. The BVS values around both Cu(1) and Cu(2) are increasing while T_c is decreasing with Ca doping. Interestingly, in most cases the BVS around Cu(1) is smaller than the BVS around Cu(2). These results are discussed in section 4.

4. Discussion

With neutron diffraction we found an initial occupancy of the 'off-chain' O(5) site ($x = 0$) corresponding to the results reported by Guillaume *et al* for R-123 (R = rare-earth elements) [21]. The occupancy of the O(5) position increases and the occupancy of the O(4) position decreases with increasing Ca content. This means that the O(4) oxygens show a tendency to partially disorder onto the O(5) sites with increasing Ca content. In the samples quenched from higher temperatures, this is less likely to happen. The slow cooling of our samples allowed us to achieve near-equilibrium conditions [24, 25]. From the Rietveld refinement of our neutron diffraction data we found no evidence that Ca^{2+} at a Y^{3+} site would prefer sixfold instead of eightfold coordination [8].

Our diffraction results show that Ca incorporation in the orthorhombic phase leads to a change of the unit-cell parameters in such a way that the orthorhombic strain decreases almost linearly up to the highest doping concentration (figure 2). This result is in

Table 4. Bond valence sums V at 1.5 K calculated using the formula (1) defined by Brown and Altermatt [13, 14].

	Bond valence sums					
x (%)	Y	Ca	Ba	Cu(1)	Cu(2)	$\sum$ cations
0 [22]	2.905(7)	—	2.192(7)	2.378(7)	2.209(1)	14.08(3)
0	2.871(4)	—	2.241(2)	2.168(4)	2.167(2)	13.85(2)
2	2.871(4)	2.529(3)	2.228(2)	2.135(4)	2.167(2)	13.79(2)
4	2.875(4)	2.532(3)	2.237(2)	2.143(4)	2.170(2)	13.82(2)
5	2.864(4)	2.522(3)	2.239(2)	2.163(4)	2.169(2)	13.83(2)
7	2.848(4)	2.508(4)	2.226(3)	2.144(5)	2.165(2)	13.75(2)
9	2.845(4)	2.505(3)	2.240(2)	2.160(4)	2.173(2)	13.80(2)
10	2.820(5)	2.484(5)	2.232(4)	2.158(7)	2.167(2)	13.74(2)
12	2.835(4)	2.497(4)	2.234(3)	2.137(5)	2.175(2)	13.75(2)
14	2.824(4)	2.487(4)	2.246(3)	2.178(5)	2.171(2)	13.79(2)
15	2.829(4)	2.492(3)	2.240(3)	2.150(5)	2.176(2)	13.76(2)
17	2.822(4)	2.485(4)	2.232(3)	2.171(6)	2.170(2)	13.74(2)
20	2.801(4)	2.467(4)	2.249(3)	2.172(5)	2.179(2)	13.76(2)

	Bond valence sums					
x (%)	O(1)	O(2)	O(3)	O(4)	O(5)	$\sum$ anions
0 [22]	2.015(4)	2.030(3)	2.014(4)	1.798(1)	—	13.83(2)
0	2.018(3)	2.027(2)	2.008(2)	1.826(2)	1.870(2)	13.99(1)
2	2.000(3)	2.029(2)	2.011(2)	1.795(2)	1.837(2)	13.91(2)
4	1.981(3)	2.031(2)	2.013(3)	1.768(2)	1.808(2)	13.91(2)
5	2.008(3)	2.027(2)	2.009(2)	1.804(2)	1.846(2)	13.96(2)
7	2.021(4)	2.023(2)	2.004(3)	1.824(2)	1.869(2)	13.91(2)
9	2.003(3)	2.028(2)	2.009(2)	1.791(2)	1.832(2)	13.92(2)
10	2.050(5)	2.019(3)	2.000(4)	1.863(3)	1.910(2)	13.95(2)
12	1.993(4)	2.026(2)	2.007(3)	1.779(2)	1.818(2)	13.84(2)
14	2.017(4)	2.023(2)	2.004(3)	1.807(2)	1.850(2)	13.96(2)
15	1.991(3)	2.029(2)	2.010(3)	1.767(2)	1.807(2)	13.87(2)
17	2.011(4)	2.029(3)	2.011(3)	1.782(2)	1.823(2)	13.91(2)
20	1.991(4)	2.027(2)	2.009(3)	1.763(2)	1.800(2)	13.88(2)

contradiction to reference [8], reporting no obvious change of the lattice parameters and of the orthorhombic strain. The increase of c with an increasing Ca content is a steric consequence of the replacement of the Y^{3+} ion (ionic radius $r = 1.019$ Å) with the larger Ca^{2+} ion ($r = 1.12$ Å) [26]. The b-axis contracts as a function of Ca substitution due to a decrease of the O(4) occupancy. The starting occupancy of the O(5) position explains the slow increase in a. The change of occupancy of the O(4) and O(5) positions and of the order of the single chains respectively are in good agreement with the decrease of orthorhombic strain with increasing substitution level.

Atomic displacements due to Ca substitution are reflected in the changes of bond lengths. A selection of atomic distances are given in table 5. Figure 8 displays the evolution of the distance between Y(Ca) and the average oxygen position of two adjacent CuO_2 planes. Obviously, an increased separation of adjacent oxygen layers is forced due to the replacement of Y^{3+} with the larger Ca^{2+}. This is not only an ion-size effect, but also caused by the reduced charge of Ca^{2+} at the Y^{3+} site. The lower positive charge at the Y site leads to two effects in the CuO_2 planes. Firstly, it diminishes the electrostatic attraction between Y(Ca) and the oxygen atoms in the adjacent CuO_2 planes. Secondly, the

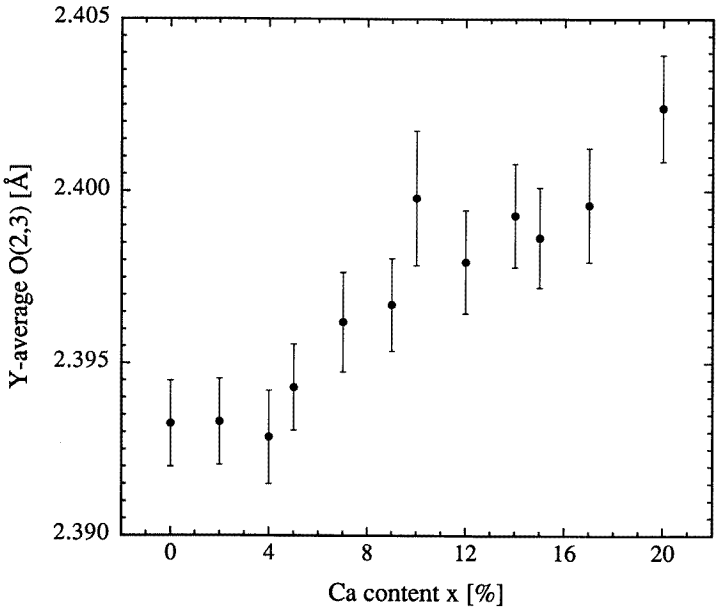

Figure 8. The distance between Y(Ca) and the average oxygen position of two adjacent CuO_2 planes of $Y_{1-x}Ca_xBa_2Cu_3O_{7-\delta}$, which is increased if calcium replaces the smaller yttrium.

electrostatic repulsion between Cu(2) and $Y^{3+}(Ca^{2+})$ is smaller. To compensate for these two effects electrostatically, the Cu(2)–Cu(2) distance of adjacent CuO_2 planes is reduced and the oxygen atoms O(2) and O(3) of the CuO_2 planes are shifted toward Cu(2) and Ba. Consequently, the buckling of the CuO_2 plane is decreasing. A further reason for the reduction of the buckling is the shift of Ba^{2+} towards the CuO_2 plane. This is expressed in the decreasing distances to the plane oxygens O(2) and O(3). The shrinking of the distance Y(Ca)–Ba might be explained by a reduced electrostatic repulsion between these cations due to the reduced charge at the Y^{3+} site produced by Ca^{2+} substitution. Due to the opposite displacement of the Ba and apical oxygen O(1), the buckling of the Ba–O(1) layer increases with decreasing Ca content.

Atomic displacements due to Ca substitution lead not only to a change of bond lengths, but also to a change of the coordination polyhedra of the cations. One has to take into account the fact that the calculated bond valence sums reflect only structural changes. Replacing Y^{3+} with the larger Ca^{2+} ion introduces internal strain in the structure. Calculation of the bond valence sums allows us to estimate the internal stress on the coordination polyhedra of the cations [27] and to determine the charges in the bond. For the cations Y^{3+} and Ca^{2+} we found decreasing bond valence sums with Ca doping. The quite high values of BVS for Ca can be explained mainly by geometric stress. The coordination polyhedron is too small for Ca^{2+} substituting for the approximately 10% smaller Y^{3+}. The decrease of the BVS for both Y and Ca can be interpreted as a change in geometric stress imposed by the movement of adjacent oxygens O(2) and O(3) away from Y(Ca) towards Ba. The size of the coordination polyhedron increases with Ca doping corresponding to figure 8. For Ba^{2+} the situation is not so clear. The values of the BVS seem to be almost unchanged. This is a result of the simultaneous change of the bond lengths of the atoms, which build the coordination polyhedron of Ba^{2+}. The distances Ba–O(1), Ba–O(4) and

Table 5. Atomic distances d [Å] in $Y_{1-x}Ca_xBa_2Cu_3O_{7-\delta}$ at 1.5 K, determined by neutron diffraction.

$x =$	0	0.02	0.04	0.05	0.07	0.09
$d_{Y(Ca)-O(2)}$	2.403(1)	2.405(1)	2.406(1)	2.405(1)	2.405(1)	2.407(1)
$d_{Y(Ca)-O(3)}$	2.384(1)	2.381(1)	2.379(1)	2.384(1)	2.387(2)	2.386(1)
$d_{Ba-O(1)}$	2.7342(3)	2.7350(3)	2.7344(3)	2.7344(3)	2.7358(3)	2.7345(3)
$d_{Ba-O(2)}$	2.988(2)	2.979(2)	2.976(2)	2.979(2)	2.980(3)	2.974(2)
$d_{Ba-O(3)}$	2.954(2)	2.953(2)	2.954(2)	2.951(2)	2.947(3)	2.945(2)
$d_{Ba-O(4)}$	2.862(2)	2.868(2)	2.871(2)	2.869(2)	2.870(2)	2.871(2)
$d_{Cu(1)-O(1)}$	1.857(2)	1.860(2)	1.864(2)	1.858(2)	1.855(2)	1.855(2)
$d_{Cu(1)-O(4)}$	1.9407(1)	1.9405(1)	1.9399(1)	1.9396(1)	1.9401(1)	1.9388(1)
$d_{Cu(2)-O(1)}$	2.268(2)	2.268(2)	2.270(2)	2.272(2)	2.276(3)	2.278(2)
$d_{Cu(2)-O(2)}$	1.9265(4)	1.9262(4)	1.9253(4)	1.9259(4)	1.9267(4)	1.9250(4)
$d_{Cu(2)-O(3)}$	1.9589(4)	1.9591(4)	1.9586(4)	1.9579(4)	1.9576(4)	1.9560(4)
$d_{Cu(2)-Cu(2)}$	3.396(2)	3.393(2)	3.388(2)	3.397(2)	3.395(2)	3.390(2)
$x =$	0.10	0.12	0.14	0.15	0.17	0.20
$d_{Y(Ca)-O(2)}$	2.407(2)	2.408(2)	2.408(2)	2.407(1)	2.406(2)	2.409(2)
$d_{Y(Ca)-O(3)}$	2.393(2)	2.388(2)	2.391(2)	2.391(2)	2.393(2)	2.396(2)
$d_{Ba-O(1)}$	2.7360(5)	2.7343(3)	2.7355(3)	2.7349(3)	2.7369(4)	2.7353(4)
$d_{Ba-O(2)}$	2.977(3)	2.971(3)	2.971(3)	2.968(2)	2.965(3)	2.961(3)
$d_{Ba-O(3)}$	2.941(3)	2.945(3)	2.939(3)	2.936(2)	2.931(3)	2.930(3)
$d_{Ba-O(4)}$	2.871(2)	2.872(2)	2.877(2)	2.878(2)	2.885(2)	2.883(2)
$d_{Cu(1)-O(1)}$	1.851(3)	1.856(2)	1.854(2)	1.856(2)	1.847(2)	1.853(2)
$d_{Cu(1)-O(4)}$	1.9394(1)	1.9381(1)	1.9384(1)	1.9376(1)	1.9372(1)	1.9361(1)
$d_{Cu(2)-O(1)}$	2.279(3)	2.279(3)	2.281(3)	2.284(2)	2.296(3)	2.292(3)
$d_{Cu(2)-O(2)}$	1.9269(5)	1.9249(4)	1.9257(4)	1.9249(4)	1.9255(4)	1.9247(4)
$d_{Cu(2)-O(3)}$	1.9560(5)	1.9550(4)	1.9552(4)	1.9537(4)	1.9530(4)	1.9511(4)
$d_{Cu(2)-Cu(2)}$	3.400(3)	3.387(2)	3.396(2)	3.385(2)	3.388(2)	3.382(2)

Ba–O(5) are increasing, while the distances Ba–O(2) and Ba–O(3) are decreasing due to a displacement of Ba^{2+} along the c-axis.

The bond valence sums around the planar and chain coppers are of much more interest due to the direct correlation with charge transfer and superconductivity [1, 28]. Usually, shorter bond lengths result in a higher oxidation state. Since we found shrinking bond lengths for Cu(2)–O(2), Cu(2)–O(3), Cu(1)–O(4) and Cu(1)–O(1), we expected to find increasing copper oxidation states. Indeed, we found a slight increase of the BVS for both Cu(1) in the chains and Cu(2) in the planes. The increase of the bond valence sum around Cu(1) is due to the increasing occupancy of the 'off-chain' O(5) site and the smaller occupancy of the O(4) position. Thus, for the calculation of the BVS for Cu(1) the proportion of the Cu(1)–O(5) distance, which is smaller than Cu(1)–O(4), increases and therefore we find a slight increase for the BVS for Cu(1) with Ca doping. The increase of the bond valence sum around Cu(2) is dominated by the replacement of Y^{3+} with Ca^{2+} adjacent to the CuO_2 planes. The change of distances from Cu(2) to the atoms building the coordination polyhedron of Cu(2), which is discussed above, is responsible for the smaller increase of the BVS for Cu(2). The distances Cu(2)–O(2) and Cu(2)–O(3) are decreasing, while Cu(2)–O(1) is increasing with Ca substitution. As a result the coordination polyhedron of Cu(2) becomes smaller with Ca substitution and therefore the BVS for Cu(2) increases. Since it has been realized that hole carriers in high-temperature superconductors have both copper and oxygen character [29], it is more suitable to estimate the charge distribution in

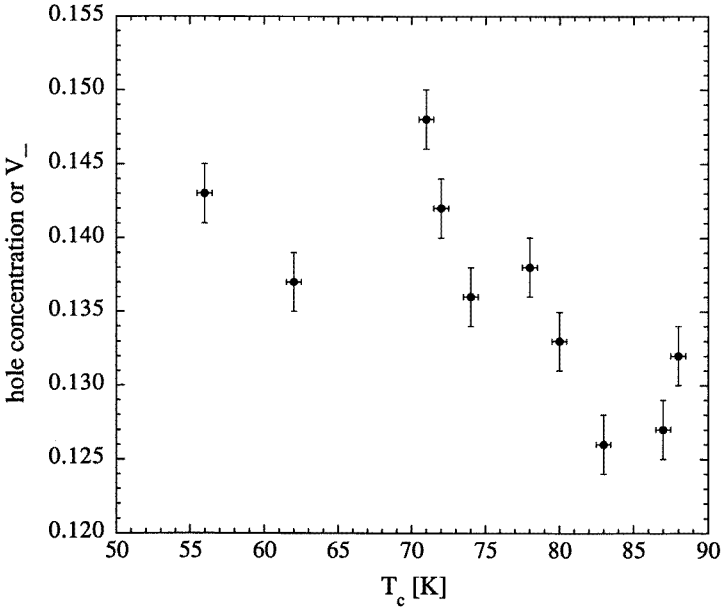

Figure 9. The bond valence sum V_- for the CuO_2 planes in $Y_{1-x}Ca_xBa_2Cu_3O_{7-\delta}$ as a function of the superconducting transition temperature T_c. The bond valence sum V_- is a measure of the hole concentration p.

terms of a combination of copper and oxygen bond valence sums. The excess charge on the Cu site is $V_{\mathrm{Cu}} - 2$ and that on the oxygen site is $2 - V_{\mathrm{O}}$. Thus the total charge on the CuO_2 planes can be estimated using the following equation given by Tallon *et al* [30]:

$$p \approx V_- = 2 + V_{\mathrm{Cu(2)}} - V_{\mathrm{O(2)}} - V_{\mathrm{O(3)}}. \tag{3}$$

Figure 9 shows the absolute hole concentration in the CuO_2 planes calculated using (3) plotted against T_c. Obviously, the absolute hole concentration in the CuO_2 planes estimated from the bond valence sum parameter V_- increases with decreasing T_c, which corresponds to an increasing Ca content. We conclude that the partial substitution for Y^{3+} with Ca^{2+} introduces additional hole carriers in the structure and makes the $Y_{1-x}Ca_xBa_2Cu_3O_{7-\delta}$ system accessible far into the overdoped region. This is in strong contradiction to the results and their interpretation given in reference [8], but in good agreement with results reported by Kontos *et al* [9] and Tallon *et al* [10].

Another result of our study supports the interpretation of overdoping of $123O_7$ with Ca substitution. For the underdoped region, Cava *et al* [22] and Jorgensen *et al* [23] have shown that the apical bond length Cu(2)–O(1) is shrinking in $YBa_2Cu_3O_{7-\delta}$ samples with increasing oxygen content and T_c. The same has been shown also for 124 under pressure [31, 32]. A shorter Cu(2)–O(1) distance facilitates the charge transfer, increases the hole concentration, and therefore increases T_c up to an optimum. For our Ca-doped $YBa_2Cu_3O_{7-\delta}$ samples we found the opposite trend in the changes of T_c and the apical bond length. The Cu(2)–O(1) distance is increased while T_c is decreased with Ca doping whereas the oxygen content remains almost unchanged. Due to this and due to the increasing of the bond valence sums around Cu(1) and Cu(2) with Ca substitution, the idea of overdoping is further confirmed.

5. Conclusions

Our systematic study on the structures of a series of polycrystalline, orthorhombic $Y_{1-x}Ca_xBa_2Cu_3O_{7-\delta}$ ($\delta < 0.04$) samples shows remarkable structural changes induced by Ca substitution. In particular, we observed the following changes with Ca doping.

(1) The distance between Y(Ca) and the oxygen O(2), O(3) of adjacent CuO_2 planes increases while the Y(Ca)–Cu(2) distance decreases with Ca doping. This is both an ion-size effect because Ca is larger than Y and an effect of the reduced charge at the Y^{3+} site produced by Ca^{2+} substitution. As a consequence, the buckling in the CuO_2 planes decreases.

(2) The Ba^{2+} ion is shifted towards the CuO_2 plane away from the single chains and therefore the buckling of the corresponding Ba–O(1) plane is increasing.

(3) The apical bond length Cu(2)–O(1) increases; this is caused by the displacements of Cu(2) towards Y(Ca) and of O(1) towards the single chain.

The latter is the most relevant structural change for the depression of superconductivity. Moreover, we found a correlation between the buckling in the CuO_2 planes and T_c. Using neutron diffraction we determined the charge distribution within the structure via measurements of the Cu–O distances and calculations of the bond valence sums. We conclude that the partial substitution for Y^{3+} with Ca^{2+} introduces additional hole carriers in the structure and makes the $Y_{1-x}Ca_xBa_2Cu_3O_{7-\delta}$ ($\delta < 0.04$) system accessible far into the overdoped region. Thus, T_c is decreasing with increasing Ca content corresponding to an increasing hole concentration in the CuO_2 planes. For $\delta \approx 0.3$ a recent neutron diffraction study [33] shows an increase of T_c as a function of Ca substitution in $Y_{1-x}Ca_xBa_2Cu_3O_{7-\delta}$, indicating that the increased number of holes may be compensated by a decrease in oxygen content.

Acknowledgments

We thank Professor A Furrer (LNS) for a critical reading of the manuscript. We are grateful to Dr H Schwer (ETH Zurich) and Professor K Bente (University of Leipzig) for critical comments on the x-ray part of our study. Funding by the Swiss National Science Foundation is also gratefully acknowledged.

References

[1] Cava R J, Batlogg B, Rabe K M, Rabe E A, Rietman E A, Gallegher P K and Rupp L W Jr 1988 *Physica* C **156** 523
[2] Miyatake T, Gotoh S, Koshizuka N and Tanaka S 1989 *Nature* **341** 419
[3] Schwer H, Kaldis E, Karpinski J and Rossel C 1994 *J. Solid State Chem.* **111** 96
[4] Buckley G, Pooke D M, Tallon J L, Presland M R, Flower N E, Staines M P, Johnson H L, Meylan M, Williams G V M and Bowden M 1991 *Physica* C **174** 383
[5] McCarron E M III, Crawford M K and Parise J B 1989 *J. Solid State Chem.* **78** 1992
[6] Chandrachood M R, Mulla I S, Gorwadkar S M and Sinha A P B 1990 *Appl. Phys. Lett.* **56** 183
[7] Greaves C and Slater P R 1989 *Supercond. Sci. Technol.* **2** 5
[8] Awana V P S and Narlikar A V 1994 *Phys. Rev.* B **49** 6353
[9] Kontos A G, Dupree R and Han Z P 1995 *Physica* C **247** 1
[10] Tallon J L, Bernhard C, Shaked H, Hitterman R L and Jorgensen J D 1995 *Phys. Rev.* B **51** 12 911
[11] STADI P STOE Powder Diffraction Software 1989 (Darmstadt)
[12] Rodríguez-Carvajal J 1993 *Physica* B **192** 55
[13] Altermatt D and Brown I D 1985 *Acta Crystallogr.* B **41** 240

[14] Brown I D and Altermatt D 1985 *Acta Crystallogr.* B **41** 244
[15] Conder K, Rusiecki S and Kaldis E 1989 *Mater. Res. Bull.* **24** 581
[16] Kosuge M, Okai B, Takahashi K and Ohta M 1988 *Japan. J. Appl. Phys.* **27** L1022
[17] Sears V F 1992 *Neutron News* **3** 26
[18] Böttger G, Schwer H, Kaldis E and Bente K 1996 submitted
[19] Schwer H, private communication
[20] Böttger G, Kaldis E and Krüger C 1996 to be published
[21] Guillaume M, Allenspach P, Henggeler W, Mesot J, Roessli B, Staub U, Fischer P, Furrer A and Trounov V 1994 *J. Phys.: Condens. Matter* **6** 7963
[22] Cava R J, Hewat A W, Hewat E A, Batlogg B, Marezio M, Rabe K M, Krajewski J J, Peck W F Jr and Rupp L W Jr 1990 *Physica* C **165** 419
[23] Jorgensen J, Veal B, Crabtree G, Claus H and Kwok W 1990 *Phys. Rev.* B **41** 1863
[24] Rusiecki S, Kaldis E, Jilek E and Rossel C 1990 *J. Less-Common Met.* **164** 31
[25] Conder K, Zech D, Krüger C, Kaldis E, Keller H, Hewat A W and Jilek E 1994 *Phase Separation in Cuprate Superconductors* ed E Sigmund and K A Müllee (Berlin: Springer)
[26] Shannon R D 1976 *Acta Crystallogr.* A **32** 751
[27] Brown I D 1989 *J. Solid State Chem.* **82** 122
[28] Tallon J L 1991 *Physica* C **176** 547
[29] Capponi J J, Chaillot C, Hewat A W, Lejay P, Marezio M, Nguyen N, Raveau B, Soubeyroux J L, Tholence J L and Tournier R 1987 *Europhys. Lett.* **3** 1301
[30] Tallon J L 1990 *Physica* C **168** 85
[31] Kaldis E, Fischer P, Hewat A W, Hewat E A, Karpinski J and Rusiecki S 1989 *Physica* C **159** 668
[32] Nelmes R J, Loveday J S, Kaldis E and Karpinski J 1990 *Physica* C **172** 311
[33] Awana V P S, Malik S K and Yelon W B 1996 *Physica* C **262** 272